Controlled electron and hole trapping in $YPO_4:Ce^{3+},Ln^{3+}$ and $LuPO_4:Ce^{3+},Ln^{3+}$ (Ln=Sm, Dy, Ho, Er, Tm)

Andreas H. Krumpel,[1,*] Adrie J. J. Bos,[1] Aurélie Bessière,[2] Erik van der Kolk,[1] and Pieter Dorenbos[1]
[1]*Faculty of Applied Sciences, Delft University of Technology, Mekelweg 15, 2629 JB Delft, The Netherlands*
[2]*Laboratoire de Chimie de la Matière Condensée de Paris, ENSCP, UMR-CNRS 7574, 11 rue Pierre et Marie Curie, 75231 Paris Cedex 05, France*

(Received 13 May 2009; revised manuscript received 23 June 2009; published 10 August 2009)

A detailed and systematic electron trapping study was conducted in the scientifically important wide band-gap materials $LuPO_4$ and YPO_4 doubly doped with Ce^{3+} and Ln^{3+} (Ln=Sm, Dy, Ho, Er, Tm). By using vacuum-ultraviolet luminescence spectroscopy and detailed thermoluminescence spectroscopy it was possible to establish by two independent methods that the observed electron traps can be assigned to the Ln^{3+} codoping ions. It is shown that the associated electron trap depths are determined by the energy separation between the Ln^{2+} ground states and the bottom of the conduction band. Both methods reveal a systematic behavior of electron trap depths as a function of the type of Ln^{3+} codoping ion that can be explained by recently developed empirical models. Small differences in trap depths obtained by the two methods are discussed in the context of charge-transfer induced relaxation processes and uncertainties in glow peak analysis. Our experiments provide valuable information on $4f^n \leftrightarrow 4f^n$, $4f^n \rightarrow 4f^{n-1}5d$, $O^{2-} \rightarrow Ln^{3+}$ charge transfer and the lowest-energy PO_4^{3-} group transitions as well as electron trap depths. These transition energies allowed us to construct a complete energy-level diagram for $LuPO_4:Ln^{3+/2+}$ and $YPO_4:Ln^{3+/2+}$.

DOI: 10.1103/PhysRevB.80.085103 PACS number(s): 78.60.Kn, 78.55.−m

I. INTRODUCTION

Doubly lanthanide doped insulators like $SrAl_2O_4:Eu,Dy$,[1,2] $CaGa_2S_4:Eu^{2+},Ho^{3+}$,[3] $BaAl_2O_4:Ce^{3+},Dy^{3+}$,[4] or $CaS:Eu^{2+},Tm^{3+}$ (Ref. 5) play an important role as luminescent afterglow phosphors in applications such as traffic signs, emergency signs, safety clothes, glow-in-the-dark toys, emergency afterglow lighting, advertising, etc. The exceptionally high afterglow efficiency and the related commercial success of these materials is to a large extent determined by the detailed charge (electrons and holes) trapping mechanism that has been the subject of many investigations the past years.

Charge carrier trapping by (pairs of) lanthanide ions is determined by the location of the lanthanide (Ln) ground state (GS) and excited states relative to the valence bands (VB) and conduction bands (CB) of host materials. One of us has recently developed empirical models that describe the systematic behavior of the energy of Ln^{2+} and Ln^{3+} ground states relative to the valence and conduction band[6,7] and have provided insight in how Ln ions as pairs can work together to efficiently store and release charges.[8] These models predict, for example, that Ce^{3+} is a stable hole trap while certain other trivalent lanthanide act as stable electron traps. Ce^{3+} ions together with other Ln^{3+} codoping ions can therefore act as efficient charge trapping couples. Optically excited Ce^{3+} ions can transfer an electron to the Ln^{3+} codoping ions that can act as a stable electron trap. During heating or at room temperature the trapped electrons are transferred back to Ce generating Ce^{3+} luminescence. Detailed experimental data that are able to verify these charge trapping models are still scarce and scattered over different investigations of different doping ions in different host lattices.[9–12]

Here, we present a detailed and systematic experimental investigation into the nature of electron traps and into the relation between trap depth and the type of Ln ion in two closely related host-lattices YPO_4 and $LuPO_4$. First, in Sec. III A the x-ray excited emission properties of $LuPO_4$ and YPO_4 doubly doped with Ce^{3+} and Ln^{3+} (Ln=Sm, Dy, Ho, Er, Tm) are presented. Then in Sec. III B, from the excitation spectra, the charge-transfer energies E^{CT} (Ln^{3+}) are established that give the location of the Ln^{2+} ground-state $4f$ energy levels with respect to the valence band. The same energy levels with respect to the conduction band are established in Sec. III C using thermoluminescence analysis techniques. Finally in Sec. IV the results of the two methods are compared and interpreted with the help of the Dorenbos model.

II. EXPERIMENTAL

A. Sample preparation

The $A_{0.994}Ce_{0.003}Ln_{0.003}PO_4$ (A=Y or Lu) powders were produced using $NH_4H_2PO_4$, A_2O_3, CeF_3, and Ln_2O_3 as starting materials. The molar ratio of the starting mixture was $NH_4H_2PO_4:A_2O_3:CeF_3:Ln_2O_3=1:0.497:0.003:0.0015$. After crushing and mixing the reactants carefully the powder was pressed to a pellet, put in a Pt crucible, and heated at first with a rate of 1 °C/min to 410 °C in a programmable furnace. It was kept at this temperature for 10 h and then cooled down to room temperature. After crushing and remixing the powder it was pressed again to a pellet and heated for a second treatment with a heating rate of 5 °C/min up to 1450 °C for 10 h. The samples purity was checked by x-ray diffraction. YPO_4 and $LuPO_4$ have the tetragonal zircon structure with space-group $I4_1/amd$ (No. 141). The metal atom is coordinated by eight oxygen atoms forming a polyhedron with site symmetry D_{2d}. The phosphate group in each compound forms a distorted tetrahedron.[13] The differences

TABLE I. Characteristic parameters of YPO_4 and $LuPO_4$; r =effective ionic radius;[14] $d(R\text{-O})$ $(R=A,P)$=average interatomic distance in polyhedra of the APO_4 structures;[13] a, c=lattice parameters.[13]

APO_4	$r(A)$ (pm)	$d(A\text{-O})$ (pm)	$d(P\text{-O})$ (pm)	a (pm)	c (pm)
YPO_4	101.9	233.7	154.3	688.2	601.8
$LuPO_4$	97.7	230.3	153.4	679.2	595.4

between the two compounds in ionic radii, interatomic distances, and lattice parameters are listed in Table I.

B. Measurement techniques

For vacuum-ultraviolet (VUV) excitation measurements a water-cooled 150W deuterium lamp (model L1835, Hamamatsu) was used in combination with a vacuum monochromator (model VM 502, ARC) as an excitation source. The light emitted from the powders was detected by a photomultiplier tube (PMT) (model B2FV45/RFI, Electron Tubes Limited) combined with an appropriate filter. Excitation spectra were corrected for background and lamp spectrum (obtained with a calibrated SXUV-type Si-ultraviolet photodiode from IRD).

In the case of the x-ray excited emission studies the x-ray tube with a Cu anode was operated at 35 kV accelerating voltage and 25 mA electrical current. The emission spectrum was recorded by the help of a vacuum monochromator (model VM 504, ARC) coupled with a PMT (EMI 9426).

The transmission loss measurements were done with a RISØ system (model TL/OSL-DA-15), consisting of an automated TL/OSL reader incorporated into a 386-based computer, a turntable with 48 sample positions and a $^{90}Sr/^{90}Y$ beta source with a dose rate of 1 mGy s^{-1}. Heating rates varied from 0.1 to 5 K/s. The emitted light of each individually heated sample was detected by a PMT (model 9235QA, Electron Tubes Limited) with a Hoya U340 filter in front of it, or a high-sensitivity fiber-optic spectrometer (model QE65000, Ocean Optics) in case of the λT-contour plots. In the case of the λT-contour plots the samples were irradiated with an external ^{60}Co source with a dose rate of 4.06 kGy h^{-1}. All TL measurements were done in a nitrogen atmosphere.

III. RESULTS

A. X-ray excited emission spectra

In Figs. 1 and 2 the x-ray excited emission spectra of YPO_4, $YPO_4:Ce^{3+},Ln^{3+}$, and $LuPO_4:Ce^{3+},Ln^{3+}$ (Ln=Sm, Dy, Ho, Er, Tm) are shown with a resolution of 2 nm. All spectra of the double-doped compounds feature the known[15] $5d^1 \rightarrow 4f^1:{}^2F_{5/2}$, ${}^2F_{7/2}$ emission of Ce^{3+} at 336 and 360 nm for $LuPO_4$, and at 333 and 356 nm for YPO_4, respectively, together with the second-order bands due to the diffraction grating of the monochromator. Both the Ce^{3+} emission and the second-order bands are indicated inside Figs. 1 and 2 by dotted, vertical lines. The specific Ln^{3+} emission lines identified in each spectrum are specified in Table II. It was reported earlier that Ho^{3+} does not show luminescence in YPO_4.[16] In our measurements we still see very weak emission lines at 475, 484, and 575 nm. The two former ones were assigned to the ${}^5F_3 \rightarrow {}^5I_8$ transition, whereas the 575-nm line is attributed to the ${}^5F_4 \rightarrow {}^5I_8$ transition despite its unusual low energy.[17,18] No Ho^{3+} emission can be observed in $LuPO_4$. The emission of Er^{3+} is very weak both in the YPO_4 and the $LuPO_4$ compounds.

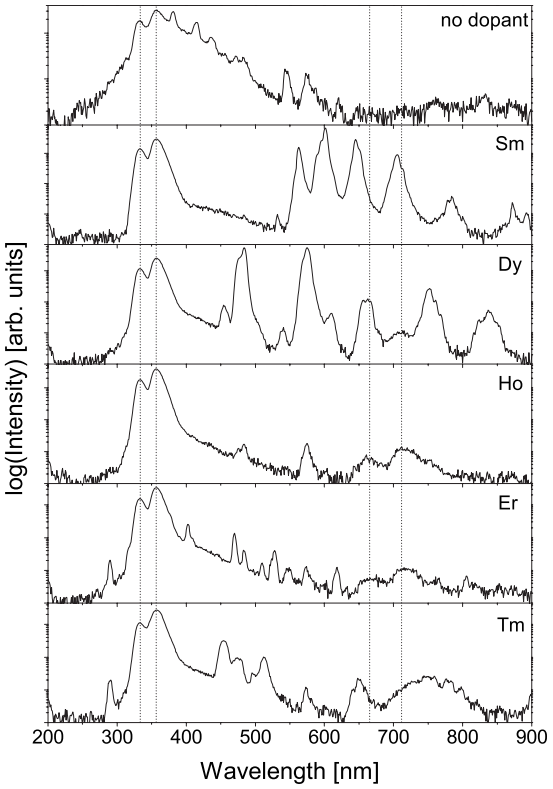

FIG. 1. Room-temperature x-ray excited emission spectra of YPO_4 and $YPO_4:Ce^{3+},Ln^{3+}$; type of Ln is specified inside each panel; the dotted vertical lines indicate both the Ce^{3+} emission (left hand) and the second-order bands of this emission (right hand); note that the spectra are displayed on a logarithmic scale.

B. VUV/UV excitation spectra

The VUV excitation spectra of YPO_4, $YPO_4:Ce^{3+},Ln^{3+}$, and $LuPO_4:Ce^{3+},Ln^{3+}$ are presented in Figs. 3 and 4. For each double-doped sample two excitation spectra were recorded: one monitoring Ce^{3+} emission and one monitoring the emission of the Ln^{3+} codopant. The identified excitation bands are summarized in Table III. The four Ce^{3+} $4f$-$5d$ transitions can be identified most easily and from there the $4f$-$5d$ transitions of all other Ln^{3+} dopants can be predicted.[19] These predictions were used in order to assign the $4f$-$5d$ excitation bands of the other Ln^{3+} dopant ions. Beside the $4f$-$5d$ excitation bands we observe broad bands that can be assigned to charge-transfer (CT) bands according to the following relation:

$$O^{2-}(2p^6) + Ln^{3+}(4f^n) \rightarrow O^{-}(2p^5) + Ln^{2+}(4f^{n+1}). \quad (1)$$

The energy of this transition, E^{CT} (Ln^{3+}), is an important parameter in the location of the Ln^{2+} $4f$ energy levels as it

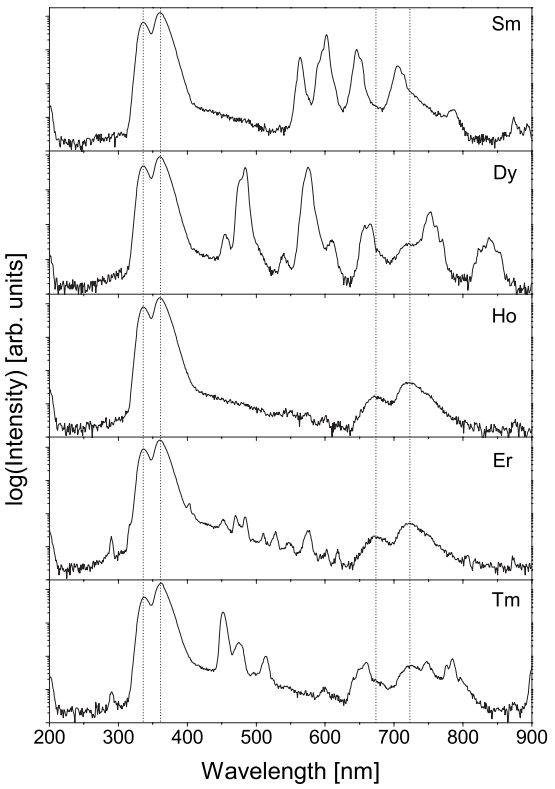

FIG. 2. Room-temperature x-ray excited emission spectra of $LuPO_4:Ce^{3+},Ln^{3+}$; type of Ln is specified inside each panel; the dotted vertical lines indicate both the Ce^{3+} emission (left hand) and the second-order bands of this emission (right hand); note that the spectra are displayed on a logarithmic scale.

can be interpreted as the energy difference between the $Ln^{2+}(4f^{n+1})$ GS and the top of the VB.[6] Van Pieterson[16,20,21] and Nakazawa[22] have studied independently of each other $YPO_4:Ln^{3+}$ and have assigned the Ln^{3+} $4f$-$5d$ and Ln^{3+} CT transitions. Their assignments are in agreement with ours (see Table III).

The excitation spectra contain as well a broadband feature at around 150 nm (open black circles). In addition, the excitation spectrum of pure YPO_4 (top panel of Fig. 3) shows a strong drop in excitation intensity at about the same wavelength. In line with the observations of Nakazawa and Shiga[22] we assign this transition to excitation of individual PO_4^{3-} groups.

When looking carefully at the excitation spectra monitoring Ln^{3+} emission it can be seen that the top of the band which was identified as the lowest PO_4^{3-} group transition energy, $E(PO_4^{3-},Ln^{3+})$, depends on the Ln^{3+} size. From Fig. 5 two observations can be made: (i) $E(PO_4^{3-},Ln^{3+})$ is larger in $LuPO_4:Ce^{3+},Ln^{3+}$ than in $YPO_4:Ce^{3+},Ln^{3+}$, and (ii) $E(PO_4^{3-},Ln^{3+})$ increases linearly with increasing Ln^{3+} ionic radius. That the host excitation energy can, in principle, be affected by the activator is understandable when we bring to mind that we look at the emission of the activator, i.e., we single out in the excitation spectra these PO_4^{3-} ions which are close enough to the activators in order to transfer the excitation energy ($PO_4^{3-} \rightarrow Ln^{3+}$). Let us discuss the two problems one by one. (i) We start with the observation that $E(PO_4^{3-},RE^{3+})$ is larger for $LuPO_4$ than for YPO_4. In the xenotime structure of $REPO_4$ (RE=Y, Lu), oxygen atoms coordinate to two rare earth (RE) and one P atom.[23] This means that not only the P^{5+} ions but also the RE^{3+} ions have, due to their size and their Coulomb potential, an effect on the stabilization of the valence electrons of the oxygen ions that are involved in the PO_4^{3-} group transition: the smaller the RE^{3+} ions and the higher their charge, the higher the binding energy of the RE^{3+}-O^{2-} system will be and the more energy will be needed in order to remove an electron from these oxygen ions. This explains why $E(PO_4^{3-},RE^{3+})$ is in general larger in $LuPO_4:Ln^{3+}$ than in $YPO_4:Ln^{3+}$. (ii) The other observation might look puzzling in the light of the previous explanation: the larger the codopant ion and the lesser its charge, the larger $E(PO_4^{3-},RE^{3+})$ when monitoring the emission of the codopant. If the activator ion is larger than the host-lattice cation which it replaces (Y or Lu), the environment of the activator will expand and affect neighboring PO_4^{3-} ions. In fact, here only the activator's environment changes while the specific interatomic arrangement of the compound remains the same at large. The increased distance between the tetrahedral PO_4 groups and the activator apparently affects the energy levels of the PO_4^{3-} ions otherwise and results in larger stabilization of the oxygen ions.

C. Thermoluminescence studies

Figure 6 displays the wavelength-resolved TL glow curves of $LuPO_4:Ce^{3+},Ln^{3+}$ in a two-dimensional λT-contour plot. Such a type of measurement is able to identify the nature of the emission during the TL process and can be used to select proper optical filters to selectively monitor emission from specific ions like Ce^{3+}. All contour plots, except the ones for $LuPO_4:Ce^{3+},Ho^{3+}$ and maybe $LuPO_4:Ce^{3+},Er^{3+}$, show the typical $5d$-$4f$ emission of Ce^{3+} at a specific temperature that is characteristic for each Ln dopant, even though it is not very intense. For $LuPO_4:Ce^{3+},Sm^{3+}$ and $LuPO_4:Ce^{3+},Dy^{3+}$ also emission from the Ln ion can be observed. These results are similar to the ones found in $YPO_4:Ce^{3+},Ln^{3+}$.[8] In contrast to $YPO_4:Ce^{3+},Ln^{3+}$, however, $LuPO_4:Ce^{3+},Ln^{3+}$ (Ln=Sm, Ho, Er) show also broadband emission around 450 nm which is probably host related.

The TL glow curves of $LuPO_4:Ce^{3+},Ln^{3+}$ both after beta irradiation and after illumination with light are shown in Fig. 7. They are similar to the glow curves of $YPO_4:Ce^{3+},Ln^{3+}$ presented in Ref. 8. The Ln^{3+}-related glow peaks that were observed in $YPO_4:Ce^{3+},Ln^{3+}$ (Ref. 8) show up as well in $LuPO_4:Ce^{3+},Ln^{3+}$ at about the same temperatures. Beside these peaks additional peaks can be noticed in all glow curves with one common peak with maximum TL intensity at about 161 °C which is assumed to be host related. In the case of $LuPO_4:Ce^{3+},Tm^{3+}$ the Tm^{3+}-related TL peak appears at similar temperatures as other host-related peaks which are also present in $LuPO_4:Ce^{3+},Er^{3+}$. In view of the detailed glow curve analysis reported for $YPO_4:Ce^{3+},Tm^{3+}$ (Ref. 8) we tentatively assigned the maximum of the broadband at 340 C to a Tm^{3+}-related glow peak. Figure 6 shows that the Dy-related glow peak in $LuPO_4:Ce^{3+},Dy^{3+}$ shows the high-

TABLE II. $5d$-$4f$ and $4f$-$4f$ transitions identified in the x-ray excited emission spectra shown in Figs. 1 and 2.

		Wavelength (nm)	
Ln	Transition	$YPO_4:Ce^{3+},Ln^{3+}$	$LuPO_4:Ce^{3+},Ln^{3+}$
Ce	$5d^1 \rightarrow 4f^1:{}^2F_{5/2}$	333	336
	$5d^1 \rightarrow 4f^1:{}^2F_{7/2}$	356	360
Sm	$4f^5:{}^4G_{5/2} \rightarrow {}^6H_{5/2}$	563	564
	${}^4G_{5/2} \rightarrow {}^6H_{7/2}$	586–611	586–611
	${}^4G_{5/2} \rightarrow {}^6H_{9/2}$	639–655	639–663
	${}^4G_{5/2} \rightarrow {}^6H_{11/2}$	694–722	694–722
	${}^4G_{5/2} \rightarrow {}^6H_{13/2}$	775–792	780–791
	${}^4G_{5/2} \rightarrow {}^6H_{15/2} + {}^6F_{1/2,3/2}$	871–893	873–893
Dy	$4f^9:{}^4F_{9/2} \rightarrow {}^6H_{15/2}$	454, 476, 484	454, 476, 484
	${}^4F_{9/2} \rightarrow {}^6H_{13/2}$	541, 575, 610	540, 575, 610
	${}^4F_{9/2} \rightarrow {}^6H_{11/2}$	646–676	646–676
	${}^4F_{9/2} \rightarrow {}^6H_{9/2} + {}^6F_{11/2}$	735–769	738–769
	${}^4F_{9/2} \rightarrow {}^6H_{7/2} + {}^6H_{9/2}$	818–855	818–858
Ho	$4f^{10}:{}^5F_3 \rightarrow {}^5I_8$	475, 484	no emission observed
	${}^5F_4 \rightarrow {}^5I_8$	575	no emission observed
Er	$4f^{11}:{}^2D_{5/2},{}^2D_{7/2} \rightarrow {}^4I_{15/2}$	290	290
	${}^2K_{3/2} \rightarrow {}^4I_{15/2}$	316	316
	${}^2H_{9/2} \rightarrow {}^4I_{15/2}$	402, 409	403, 409
	${}^4F_{5/2} \rightarrow {}^4I_{15/2}$	no emission observed	448–456
	${}^4F_{7/2} \rightarrow {}^4I_{15/2}$	470, 483	470, 484
	${}^4G_{11/2} \rightarrow {}^4I_{13/2}$	510, 512	510–513
	${}^2H(2)_{11/2} \rightarrow {}^4I_{15/2}$	521–528	524–531
	${}^4S_{3/2} \rightarrow {}^4I_{15/2}$	543–553	544–553
	${}^2H_{9/2} \rightarrow {}^4I_{13/2}$	569–580	569–575
Tm	$4f^{12}:{}^1I_6 \rightarrow {}^3H_6$	291	291
	${}^1D_2 \rightarrow {}^3F_4$	454	452
	${}^1G_4 \rightarrow {}^3H_6$	474	475
	${}^1D_2 \rightarrow {}^3H_5$	495, 512	496, 513
	${}^1G_4 \rightarrow {}^3F_4 + {}^1D_2 \rightarrow {}^3H_4$	641, 648, 659	641, 648, 660
	${}^1G_4 \rightarrow {}^3H_5 + {}^1D_2 \rightarrow {}^3F_3$	759–798	748–796

est TL intensity among all Ln-related glow peaks. This fact has also been observed in $YPO_4:Ce^{3+},Ln^{3+}$ (Ref. 8) and $NaLaF_4:Ce^{3+},Ln^{3+}$.[24]

Following Bos and Dorenbos,[8] we have determined the activation energy, E_A, from each Ln-related glow peak shown in Fig. 7 with three different methods assuming in all cases first-order kinetics, i.e., neglecting retrapping during heating.

(i) First we have used a simple formula of the form[25]

$$E_A = 2.52 \cdot k_B T_m^2/\mathrm{FWHM} - 2k_B T_m, \tag{2}$$

where k_B (eV/K) is the Boltzmann constant, T_m (K) the temperature at which the glow peak has maximum intensity, and FWHM means the full width at half maximum of the glow peak.

(ii) The second method makes use of the dependence of T_m on the heating rate, β (K/s). In first-order kinetics the condition for maximum TL intensity can be written as an Arrhenius equation,[25]

$$\ln(T_m^2/\beta) = E_A/k_B T_m + \ln(E_A/k_B s), \tag{3}$$

in which s (s^{-1}) indicates the frequency factor. Plotting Eq. (3) against $1/k_B T_m$ (heating rate plots) results in a straight line with slope E_A and intercept $\ln(E_A/k_B s)$. The heating rate plots for all $LuPO_4:Ce^{3+},Ln^{3+}$ samples are shown in Fig. 8.

(iii) Finally, as third method, we have analyzed each glow peak by the help of a program called GLOWFIT.[26] An example of such a fit is given in Fig. 9. The activation energies determined with these three methods are displayed together with the predicted values given by the Dorenbos model[27] in Table IV.

The values given in columns 2 and 4 of Table IV are the arithmetic mean of all measured glow curves with different

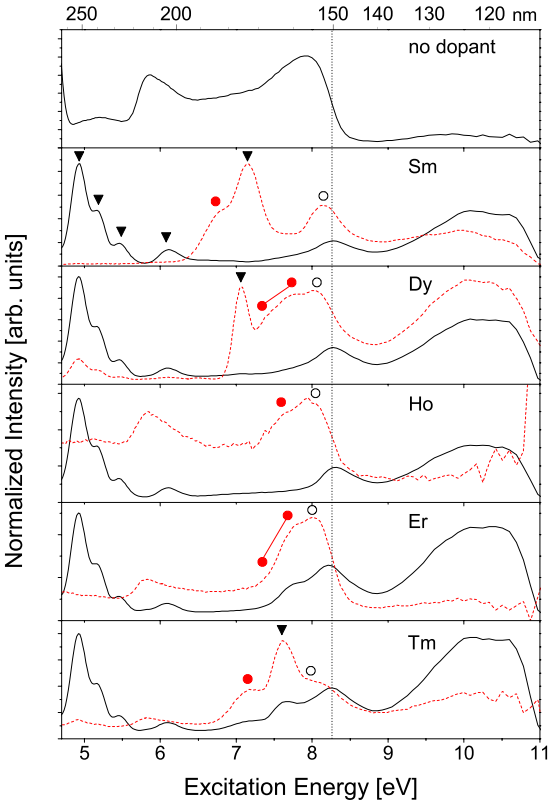

FIG. 3. (Color online) Room-temperature VUV excitation spectra of YPO_4 and YPO_4:Ce^{3+},Ln^{3+} monitoring Ce^{3+} emission (solid line) and Ln^{3+} emission (dashed line); in the case of pure YPO_4 the broadband emission around 350 nm has been monitored; type of Ln is specified inside each panel; inside the panels also the band positions of $4f$-$5d$ (black triangle) transitions, $O^{2-} \rightarrow Ln^{3+}$ CT transitions (filled circles) and the lowest PO_4^{3-} group transition (open circles) are shown. The line at about 8.27 eV indicates the lowest PO_4^{3-} group transition monitoring Ce^{3+} emission.

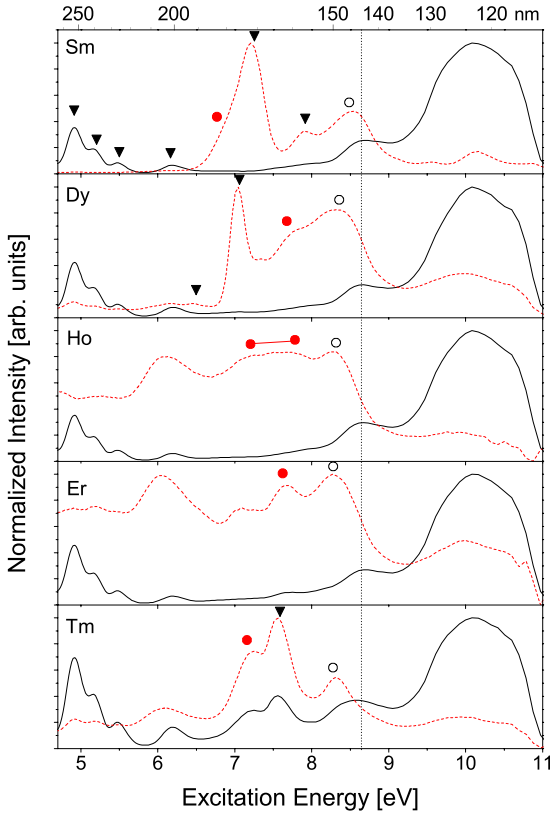

FIG. 4. (Color online) Room-temperature VUV excitation spectra of $LuPO_4$:Ce^{3+},Ln^{3+} monitoring Ce^{3+} emission (solid line) and Ln^{3+} emission (dashed line); type of Ln is specified inside each panel; inside the panels also the band positions of $4f$-$5d$ (black triangle) transitions, $O^{2-} \rightarrow Ln^{3+}$ CT transitions (filled circles) and the lowest PO_4^{3-} group transition (open circles) are shown. The line at about 8.6 eV indicates the lowest PO_4^{3-} group transition monitoring Ce^{3+} emission.

heating rates together with the standard deviation. The values in column 3 of Table IV represent the slope and the standard deviation of the least-squares fit of the straight line to the single data points. Each data point was taken from one glow curve with a specific heating rate.

IV. DISCUSSION

One main objective of this section is to derive energy-level diagrams of both YPO_4:Ln^{3+} and $LuPO_4$:Ln^{3+} in which we place the Ln^{2+} ground states of all the Ln^{2+} doping ions with respect to the conduction and valence bands of the YPO_4 and $LuPO_4$ hosts. First, we will derive the band-gap energy from the luminescence excitation spectra (Sec. IV A). Second, we place the Ln^{2+} ground-state levels with respect to the top of the valence band using the observed CT transitions (Sec. IV B). Third, we place the Ln^{2+} ground-state levels relative to the conduction-band edge on the bases of the TL data (Sec. IV C). Finally, we present and discuss the resulting energy-level diagram as presented in Fig. 11 (Sec. IV D).

A. Estimation of exciton creation and band-gap energy

The first allowed PO_4^{3-} group transition energy, $E(PO_4^{3-},RE^{3+})$, can be considered as the minimum energy needed to create a bound exciton. The abbreviation RE (rare earth=lanthanides+Y and Sc) has been included in the definition of this energy as the rare-earth ion of the host as well as the Ln dopant has an effect on it (see Fig. 5). The exciton creation energy is somewhat smaller than the band-gap energy, E_{VC}, i.e., the minimum energy needed to make a free electron and a free hole. Furthermore, we consider E_{VC} the energy between the top of the valence band and the bottom of the conduction band (band gap). We have chosen to use the following simple relation between exciton energy and band-gap energy:

$$E_{VC} \cong 1.05 \cdot E(PO_4^{3-},RE^{3+}). \quad (4)$$

With Eq. (4) we assume the difference between $E(PO_4^{3-},RE^{3+})$ and E_{VC} to be about 2% smaller than stated by Dorenbos for oxide compounds.[7] This smaller distance has been chosen in order to bring the energetic locations of the Ln^{2+}:$4f^{n+1}$ ground states set by the activation energies of the Ln-related TL glow peaks and the Ln^{3+} CT energies into an optimal agreement.

From the excitation spectrum of pure YPO_4 (see Fig. 3), $E(PO_4^{3-},Y^{3+})$ was identified to be 8 eV (155 nm). This is in agreement with the value that would have been expected

TABLE III. $4f$-$5d$ and $O^{2-} \rightarrow Ln^{3+}$ CT energies identified in the VUV excitation spectra shown in Figs. 3 and 4.

		Energy (eV)	
Ln	Transition	$YPO_4:Ce^{3+},Ln^{3+}$	$LuPO_4:Ce^{3+},Ln^{3+}$
Ce	$4f \rightarrow 5d^1$	4.93, 5.19, 5.46, 6.1	4.92, 5.19, 5.48, 6.2
Sm	$4f \rightarrow 5d^1$	7.15	7.24, 7.9
	$O^{2-} \rightarrow Sm^{3+}$ CT	6.75	7.0
Dy	$4f \rightarrow 5d^1$	6.49 (s.f.), 7.06 (s.a.)	6.45 (s.f.), 7.05 (s.a.)
	$O^{2-} \rightarrow Dy^{3+}$ CT	7.34–7.74	7.57–7.84
Ho	$O^{2-} \rightarrow Ho^{3+}$ CT	7.6	7.2–7.78
Er	$O^{2-} \rightarrow Er^{3+}$ CT	7.32–7.76	7.65
Tm	$4f \rightarrow 5d^1$	7.6	7.56
	$O^{2-} \rightarrow Tm^{3+}$ CT	7.05–7.24	7.07–7.24

based on the linear relation between $E(PO_4^{3-},RE^{3+})$ and $r(RE^{3+})$ which is displayed in Fig. 5, taking $r(Y^{3+})$ =101.9 pm.[14] In view of this linear relation the corresponding transition energy in $LuPO_4$, $E(PO_4^{3-},Lu^{3+})$, was estimated to be at about 8.22 eV (151 nm), for $r(Lu^{3+})$ =97.7 pm.[14] Nakazawa specifies this energy with 8.55 eV (145 nm).[22] Using formula (2) it is now possible to estimate the band-gap energies of YPO_4 and $LuPO_4$ at 8.4 and 8.63 eV, respectively. These values were used in Fig. 10.

B. Charge transfer transitions

Figure 10 shows the two energy-level diagrams of $YPO_4:Ce^{3+},Ln^{3+}$ and $LuPO_4:Ce^{3+},Ln^{3+}$. It will be discussed in the following step-by-step procedure on how they have been constructed.

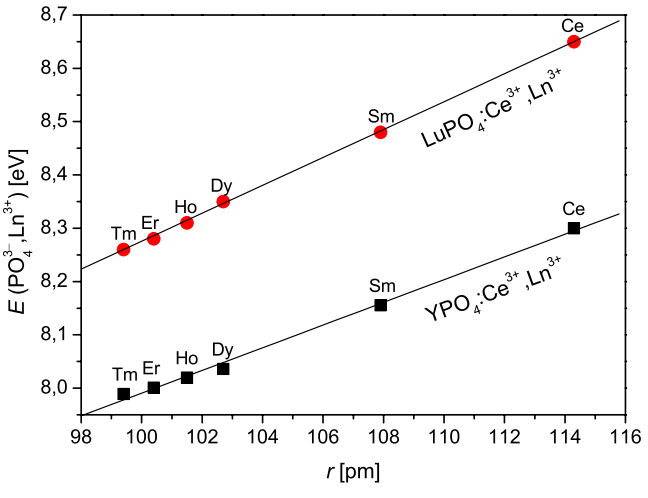

FIG. 5. (Color online) Lowest PO_4^{3-} group transition energy, $E(PO_4^{3-},Ln^{3+})$, in $YPO_4:Ce^{3+},Ln^{3+}$ and $LuPO_4:Ce^{3+},Ln^{3+}$ as a function of the effective atomic radius, r, of the Ln^{3+} codopant and Ce^{3+}; $E(PO_4^{3-},Ln^{3+})$ is taken from the VUV excitation spectra presented in Figs. 3 and 4 monitoring Ce, Sm, Dy, Ho, Er, or Tm emission; type of Ln^{3+} emission is specified inside the figure.

$O^{2-} \rightarrow Ln^{3+}$ charge-transfer transitions (see Eq. (1)) give direct information about the energy of the Ln^{2+} ground states relative to the top of the VB.[6] Provided the energy difference between the VB and CB band is known (see Sec. IV A.) it is possible to position the Ln^{2+} GS energies relative to the CB as well. The filled circles in Figs. 3, 4, and 10 indicate the $O^{2-} \rightarrow Ln^{3+}$ CT transitions which are summarized in Table III. These CT transitions give approximately the $Ln^{2+}:4f^{n+1}$ ground states relative to the top of the VB.[6] The open circles in Fig. 10 are predictions by the Dorenbos model which claims a constant, i.e., host-independent energy difference between two neighboring $4f$ ground states inside the energy-level diagram both for the divalent and the trivalent Ln dopant ions. The experimentally determined CT energies combined with the Dorenbos model allow one to predict immediately that Sm^{3+}, Dy^{3+}, Ho^{3+}, Er^{3+}, and Tm^{3+} are stable electron traps in these phosphate hosts as their Ln^{2+} $4f$ GS is located below the bottom of the CB. In addition the expected trap depths can be derived. In Sec. IV D we will compare and discuss the electron trap depth with those obtained from TL measurements. For Ce^{3+} the situation is not as clear as it might appear. Although the $Ce^{2+}:4f^2$ GS is energetically located inside the CB and, hence, cannot trap an electron, the $5d$ levels of Ce^{2+} could be located below the bottom of the CB. In that case Ce^{3+} could still trap an electron. We can demonstrate with few thoughts that this is not the case: both in $YPO_4:Ce^{3+}$ and in $LuPO_4:Ce^{3+}$ the lowest Ce^{3+} $4f$-$5d$ transition occurs at about 30,800 cm^{-1} (325 nm).[15,20] For the free Ce^{3+} ion the lowest $4f$-$5d$ transition was found to be at about 201 nm.[28] That means that the crystal-field depression or redshift for the trivalent lanthanides, $D(A,Ln^{3+})$, i.e., the energy difference between the Ce^{3+} $4f$-$5d$ transition energy of the free ion and the one of Ce^{3+} doped in a compound A, is approximately 2.35 eV in YPO_4 and in $LuPO_4$. From this value we can calculate the redshift for the divalent Ln ions, $D(A,Ln^{2+})$, in these two compounds to be about 1.271 eV.[29] Considering that the lowest $4f$-$5d$ transition in free Ce^{2+} is at about 2830 cm^{-1} (0.351 eV) (Ref. 30) we can say that the lowest $5d$ level of Ce^{2+} is located approximately 0.92 eV below the $4f$ GS of Ce^{2+}. Based on the energy-level diagrams shown in Fig. 10

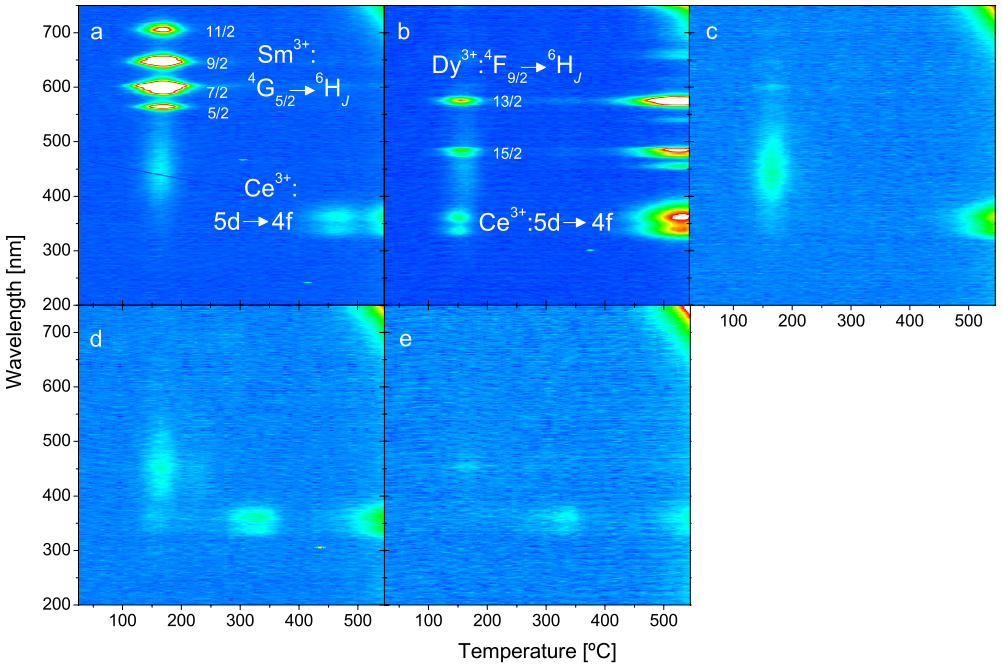

FIG. 6. (Color online) λT-contour plots of $LuPO_4:Ce^{3+},Sm^{3+}$ (a), $LuPO_4:Ce^{3+},Dy^{3+}$ (b), $LuPO_4:Ce^{3+},Ho^{3+}$ (c), $LuPO_4:Ce^{3+},Er^{3+}$ (d), and $LuPO_4:Ce^{3+},Tm^{3+}$ (e), after gamma irradiation with a dose of 4.3 kGy from a ^{60}Co source; heating rate=5 K/s.

and the estimation of the CB bottom given by Eq. (4) this would place the lowest 5*d* level of Ce^{2+} inside the CB. In that case Ce^{3+} could not be an electron trap.

It is possible to estimate the location of the Ln^{3+} ground states from the position of the Ln^{2+} ground states. It has been shown that in wide band-gap compounds the energy difference between the $4f^6$ GS energy of Eu^{3+} and the $4f^7$ GS energy of Eu^{2+} is always between 6.6 and 7.3 eV.[6,30] In Fig. 10 we have used a value of 6.6 eV for the Eu^{3+}/Eu^{2+} energy difference to place the Ln3+GS curve with respect to the Ln^{2+} GS curve. This clearly shows that the Ce^{3+} GS is energetically located inside the band gap and hence Ce^{3+} can act as a hole trap. The position of the Ln^{3+} GS is used in the next section to explain the observed charge trapping phenomena.

C. Thermoluminescence activation energies

Our choice to study $LuPO_4$ doubly doped with Ce^{3+} and a second Ln^{3+} codopant ion was motivated by a previous study on YPO_4 also doubly doped with Ce^{3+} and a second Ln^{3+} ion.[8] From that study it was concluded that after high-energy irradiation, the Ce^{3+} dopant ion gives off an electron. Conduction-band electrons on the other hand can be trapped by the Ln^{3+} codopant that are stable electron traps. We have shown in Sec. III C. that each glow curve (see Fig. 7) has Ln-related glow peaks. This means that the Ln codopants must act as charge traps. We have also shown in Sec. IV B. that the Ln codoping ions are stable electron traps. In addition to that, it was shown in Fig. 6 that the Ln-related glow peaks are mainly causing emission from Ce^{3+} that in addition can only act as a hole trap as demonstrated in the previous section. We have therefore strong indications that the charge trapping mechanism in $LuPO_4$ is the same as in YPO_4. During heating (from room temperature up to 500 °C) the

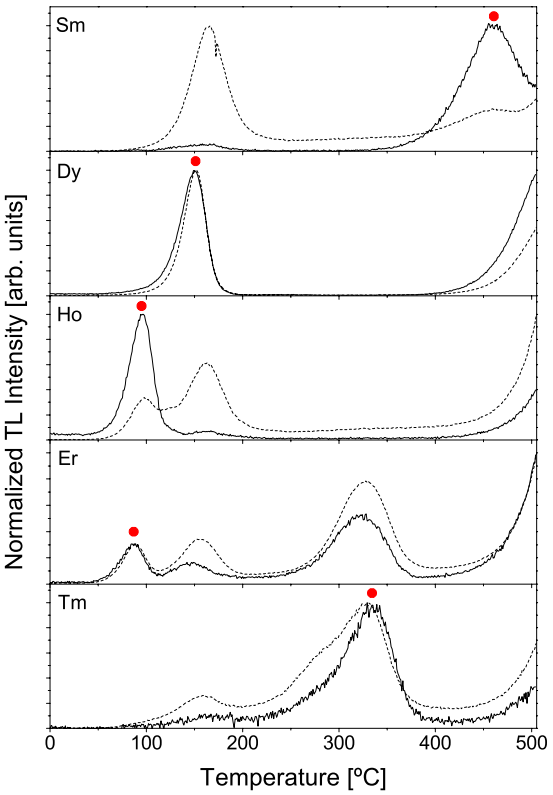

FIG. 7. (Color online) Normalized TL glow curves of $LuPO_4:Ce^{3+},Ln^{3+}$ monitoring Ce^{3+} emission after 600-mGy beta irradiation (solid line) and 30-min irradiation with deuterium lamp in ambient gas atmosphere (dashed line); heating rate=5 K/s; type of Ln is specified inside each panel; the filled circle shown in each panel indicates the glow peak due to thermally stimulated $Ln^{2+} \rightarrow Ce^{4+}$ CT.

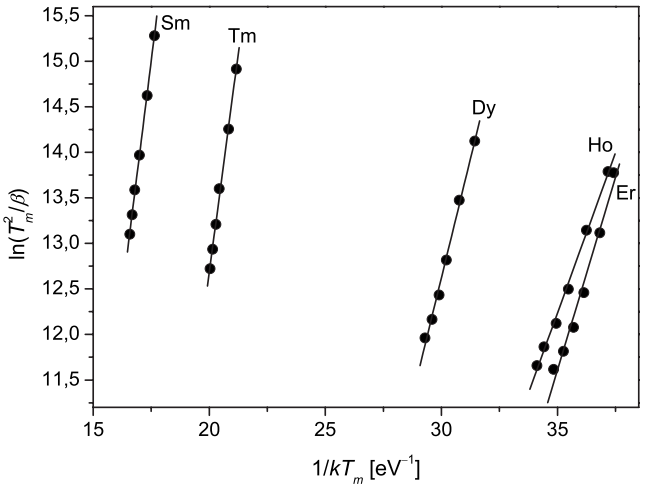

FIG. 8. Heating rate plots of the $LuPO_4:Ce^{3+},Ln^{3+}$ glow curves after beta irradiation; type of Ln is specified inside the figure.

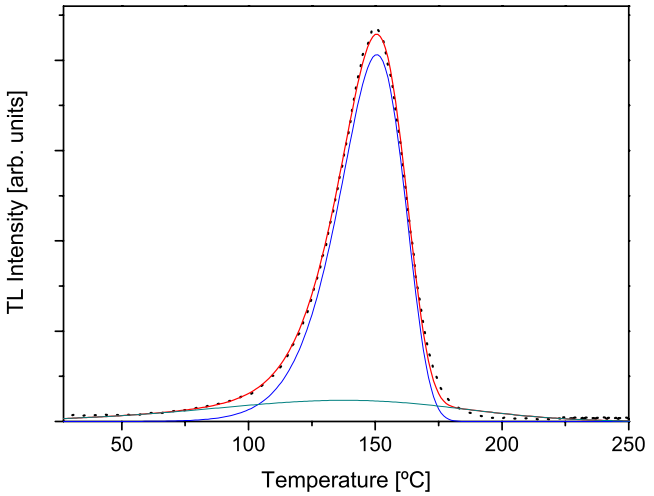

FIG. 9. (Color online) Glow curve analysis by fitting with two first-order glow peaks using the glow curve of $LuPO_4:Ce^{3+},Dy^{3+}$ after beta irradiation that is shown in Fig. 6.

trapped electron is released from the $Ln^{2+}:4f^{n+1}$ GS and recombines via the CB with Ce^{4+}. As a result of this recombination Ce^{3+} emission can be observed. Thus, in these cases where the Ln-related glow peak consists mainly (or partly in $LuPO_4:Ce^{3+},Dy^{3+}$) of Ce^{3+} emission, the charge storing mechanism can be expressed as follows:

$$Ce^{3+}(4f^1) + Ln^{3+}(4f^n) \xrightarrow{\Delta E} Ce^{4+}(4f^0) + Ln^{2+}(4f^{n+1}). \quad (5)$$

ΔE symbolizes the energy introduced into the compound in form of high-energy radiation. The charge trapping mechanism expressed in Eq. (5) predicts that identical TL glow curves are expected when electrons from Ce^{3+} are directly excited into the CB and are successively trapped by the Ln^{3+} codopant ions. This is indeed confirmed by the TL glow curves obtained after illumination with UV light (see Fig. 7). The energy which is needed to ionize Ce^{3+} in $LuPO_4$ is lower than the band-gap energy, $E(PO_4^{3-},Ln^{3+})$, and can be reached by UV light. As a light source a deuterium lamp was used and the experiment was carried out in ambient air in order to ensure that the high-energy radiation able to excite across the band gap (about 150 nm) was filtered out. Since the TL emission after UV illumination is again from Ce^{3+} and the TL glow curves look very similar to the ones obtained after beta irradiation, the mechanism expressed by Eq. (5) is confirmed. The activation energy that is needed in order to release the electron from the Ln^{2+} ground state was derived from each of the Ln-related glow peaks presented in the experimental section (see Table IV). The activation energies provide a second means to locate the Ln^{2+} ground states relative to the CB and by using the band-gap energy also relative to the VB. In Fig. 10 we have plotted the $Ln^{2+}:4f^{n+1}$ ground states relative to the top of the VB and the bottom of the CB as horizontal bars.

Finally, we discuss the origin of the TL from Dy^{3+} and Sm^{3+} in $LuPO_4:Ce^{3+},Dy^{3+}$ and $LuPO_4:Ce^{3+},Sm^{3+}$. In $LuPO_4:Ce^{3+},Dy^{3+}$ the Ln-related glow peak not only consists of emission from Ce^{3+} but also from Dy^{3+}, and $LuPO_4:Ce^{3+},Sm^{3+}$ shows Sm^{3+} emission at lower temperatures than the Sm-related glow peak. The fact that we observe Dy^{3+} and Sm^{3+} emission implies that besides Ce^{3+} also these two ions can act as recombination centers. In $LuPO_4:Ce^{3+},Dy^{3+}$ the Dy^{3+} ion can act both as hole and electron trap as its $Dy^{3+}:{}^6H_{15/2}$ as well as the $Dy^{2+}:{}^6I_8$ ground states are inside the forbidden band gap (see Fig. 10). Thus, the recombination may occur in principle either via an electron release from $Dy^{2+}:{}^6I_8$ or via a release of a hole from $Dy^{3+}:{}^6H_{15/2}$. We have discussed in another study on $NaLaF_4:Ln^{3+}$ (Ref. 24) the possibility of the formation of a V_{kA} center that might be stabilized by a host or a Ln impurity. Such a V_{kA} center can be freed thermally and can transfer the hole via a hopping mechanism to the Ln^{2+} ion producing Ln^{3+} emission. This mechanism could explain the situation in $LuPO_4:Ce^{3+},Ln^{3+}$ (Ln=Sm, Dy). But as the

TABLE IV. Mean values of the activation energies in $LuPO_4:Ce^{3+},Ln^{3+}$ derived by three different methods from the TL glow curves and activation energies derived via $E_{VC}-E^{CT}(Ln^{3+})$.

Codopant	Simple formula	Heating rate method	Glow curve analysis	$E_{VC}-E^{CT}(Ln^{3+})$
Sm	1.37 ± 0.05	2.04 ± 0.02	1.72 ± 0.06	1.6
Dy	0.93 ± 0.05	1.05 ± 0.06	1.02 ± 0.09	1.03
Ho	0.77 ± 0.04	0.70 ± 0.06	0.81 ± 0.1	0.82
Er	0.74 ± 0.03	0.85 ± 0.1	0.81 ± 0.07	0.95
Tm	1.20 ± 0.13	1.93 ± 0.06	1.32 ± 0.17	1.53

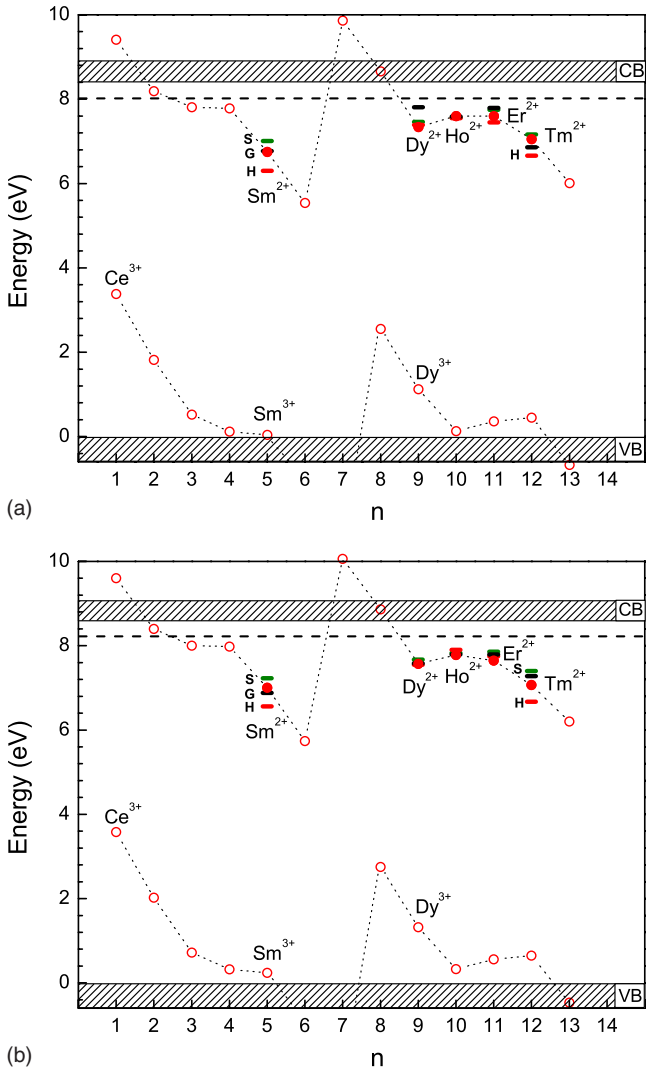

FIG. 10. (Color online) Energy-level diagrams of $YPO_4:Ln^{2+}$ (a) and $LuPO_4:Ln^{2+}$ (b); n $(n+1)$ is the number of electrons in the $4f$ shell of the trivalent (divalent) lanthanide ions. Filled circles indicate the host-dopant CT energies which have been identified in the VUV excitation spectra, whereas the open circles are prediction from the Dorenbos model. The dashed horizontal line indicates the lowest PO_4^{3-} group transition energy, $E(PO_4^{3-},Ln^{3+})$. The energy levels based on the TL activation energies derived by three methods (S=simple formula, H=heating rate method, and G=glow curve analysis) are displayed as well.

Dy^{3+} and Ce^{3+} emission is found at the same temperature in the case of $LuPO_4:Ce^{3+},Dy^{3+}$, both processes could take place at the same time only when the Dy-trapped electron and the Dy-trapped hole are characterized by approximately the same activation energies.

D. Dependence of LN^{2+} level location on experimental method

From Fig. 10 it can be concluded that the location of the Ln^{2+} ground states relative to the CB depends on the experimental method used, which is TL activation or CT energies. Three possible explanations for this behavior are given and discussed below.

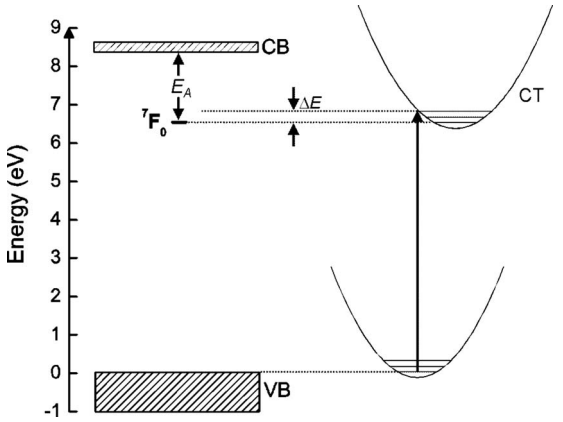

FIG. 11. Energy-level diagram (left side) and configurational coordinate diagram (right side) of $YPO_4:Sm^{3+}$; the arrow on the right-hand side indicates the $O^{2-}\rightarrow Sm^{3+}$ CT transition as used for energy-level location. Due to relaxation processes the Sm^{2+}: $^7F_0$ GS will be lowered in energy relative to the VB and the CB by an amount ΔE. The activation energy, E_A, is considered to express the energy difference between the Sm^{2+}: $^7F_0$ GS in equilibrium position and the bottom of the CB.

Fist of all, it can be seen that the activation energies which are derived by the three different TL methods explained in Sec. III C for one glow peak are not the same. In the case of Sm for instance, the activation energy derived with the simple formula is 0.67 eV lower in energy than the one derived with the heating rate method. For Dy, Ho, and Er, however, the differences are relatively small. In general it is assumed that the activation energies derived from the heating rate plots give the most reliable values.

Second, it is important to note that the Ln^{2+} GS energy as determined from TL measurements relative to the VB depends on the band-gap energy, provided that Eq. (5) holds and that the charge-carrier recombination happens via the CB. If, for example, the band gap derived by us in Sec. IV A, would be 0.1 eV larger, then this would increase the Ln^{2+} GS energies relative to the VB as well by 0.1 eV.

Third, we note that the energy locations of the Ln^{2+} ground states relative to the top of the VB as derived from CT measurements do have to be handled with care. In Fig. 11 the situation is depicted schematically both in form of an energy-level diagram and a configurational coordinate diagram. A CT transition as shown in Fig. 11 (right hand) starts from the lowest vibrational level of the GS parabola and ends on an edge of the excited-state parabola where the vibrational levels have their highest amplitude. This is the transition energy E^{CT} (Ln^{3+}) which was used by us for the GS level location of the divalent Ln ions. With this we ignore, though, the energy difference ΔE between the edge of the excited-state parabola and its lowest vibrational level, i.e., the actual Ln^{2+} GS. This equilibrium Ln^{2+} GS is the starting point of the thermally stimulated electron release mechanism.

In summary, it can be stated that level location by means of Ln^{3+} CT energies is independent from an accurate location of the CB but it ignores relaxation processes and hence gives not the energetic location of the GS in equilibrium position.

Level location by means of TL activation energies on the other hand does depend on the assignment of the CB bottom energy which may be subjected to experimental error as it is often poorly defined.

In the energy-level diagrams presented in Fig. 10 the energetic locations of the $Ln^{2+}:4f^{n+1}$ ground states set by the activation energies of the Ln-related TL glow peaks, i.e., the $E_{VC}-E_A$ values, and the Ln^{3+} CT energies, E^{CT} (Ln^{3+}), are brought into agreement best by means of Eq. (4). As already mentioned in Sec. IV B., the $4f$ energy levels of the Ln^{3+} ions that are included in the energy-level diagrams (Fig. 10) were placed with regard to the Eu^{3+}/Eu^{2+} $4f$ GS energy difference of 6.6–7.3 eV that was found in wide band-gap compounds. Our choice of 6.6 eV was done in view of the observed Dy^{3+} and Sm^{3+} emission that could be explained by assuming the hole-trapping mechanism explained in the previous section.

Despite the small uncertainties in the location of the Ln $4f$ GS energies, the energy-level diagrams are able to explain the Ln-related glow peaks an might be used in order to control TL processes and to design new TL materials with improved properties.

V. CONCLUSIONS

An experimental electron trapping and transport study on $YPO_4:Ce^{3+},Ln^{3+}$ and $LuPO_4:Ce^{3+},Ln^{3+}$ (Ln=Sm, Dy, Ho, Er, Tm) was presented and analyzed. It was concluded that after high-energy radiation or direct Ce^{3+} excitation, the Ce^{3+} dopant ion becomes a hole trap. The released electron on the other hand is trapped by the Ln^{3+} codopant. Both the $Ce^{4+}:4f^0$ and the $Ln^{2+}:4f^{n+1}$ ground states are stable at room temperature. During heating the trapped electron is thermally activated from the $Ln^{2+}:4f^{n+1}$ GS and recombines via the CB with Ce^{4+}. As a result of this recombination Ce^{3+} emission is observed. It was found that the systematic change in activation energies as a function of the type of Ln^{3+} codoping ion that was derived from the thermoluminescence glow peaks, is in good agreement with the Ln^{2+} GS energies with respect to the conduction band found via the $O^{2-}\rightarrow Ln^{3+}$ CT bands which for their part were identified in the VUV excitation spectra. Based on this analysis, energy-level diagrams for both types of compounds were constructed that might be used in order to control TL processes and to design new TL materials with improved properties.

ACKNOWLEDGMENT

This work was supported by the Dutch Technology Foundation (STW).

*Corresponding author. FAX: +31-15-27-89011; a.h.krumpel@tudelft.nl

[1] M. Kamada, J. Murakami, and N. Ohno, J. Lumin. **87-89**, 1042 (2000).
[2] Y. Kamiyanagi, M. Kitaura, and M. Kaneyoshi, J. Lumin. **122-123**, 509 (2007).
[3] C. Guo, C. Zhang, Y. Lü, Q. Tang, and Q. Su, Phys. Status Solidi A **201**, 1588 (2004).
[4] D. Jia, X. Wang, E. van der Kolk, and W. Yen, Opt. Commun. **204**, 247 (2002).
[5] D. Jia, W. Jia, D. Evans, W. Dennis, H. Liu, J. Zhu, and W. Yen, J. Appl. Phys. **88**, 3402 (2000).
[6] P. Dorenbos, J. Phys.: Condens. Matter **15**, 8417 (2003).
[7] P. Dorenbos, J. Lumin. **111**, 89 (2005).
[8] A. J. J. Bos and P. Dorenbos, Radiat. Meas. **43**, 222 (2008).
[9] Z. Qi, C. Shi, M. Liu, D. Zhou, X. Luo, J. Zhang, and Y. Xie, Phys. Status Solidi A **201**, 3109 (2004).
[10] F. Clabau, X. Rocquefelte, S. Jobic, P. Deniard, M. H. Whangbo, A. Garcia, and T. Le Mercier, Solid State Sci. **9**, 608 (2007).
[11] J. Hölsä, T. Aitasalo, H. Jungner, M. Lastusaari, J. Niittykoski, and G. Spano, J. Alloys Compd. **374**, 56 (2004).
[12] O. Arellano-Tanori, R. Melendrez, M. Pedroza-Montero, B. Castanedea, V. Chernov, W. M. Yen, and M. Barboza-Flores, J. Lumin. **128**, 173 (2008).
[13] W. O. Milligan and D. F. Mullica, Inorg. Chim. Acta **60**, 39 (1982).
[14] R. D. Shannon, Acta Crystallogr., Sect. A: Cryst. Phys., Diffr., Theor. Gen. Crystallogr. **32**, 751 (1976).
[15] E. Nakazawa and S. Shionoya, J. Phys. Soc. Jpn. **36**, 504 (1974).
[16] L. van Pieterson, Ph.D. thesis, Proefschrift Universiteit Utrecht, 2001.
[17] I. K. Battisha, J. Sol-Gel Sci. Technol. **30**, 163 (2004).
[18] J. Li, J. Wang, H. Tan, X. Cheng, F. Song, H. Zhang, and S. Zhao, J. Cryst. Growth **256**, 324 (2003).
[19] P. Dorenbos, J. Lumin. **91**, 91 (2000).
[20] L. van Pieterson, M. F. Reid, R. T. Wegh, S. Soverna, and A. Meijerink, Phys. Rev. B **65**, 045113 (2002).
[21] L. van Pieterson, M. F. Reid, G. W. Burdick, and A. Meijerink, Phys. Rev. B **65**, 045114 (2002).
[22] E. Nakazawa and F. Shiga, J. Lumin. **15**, 255 (1977).
[23] Y. Ni, J. M. Hughes, and A. N. Mariano, Am. Mineral. **80**, 21 (1995).
[24] A. H. Krumpel, E. van der Kolk, D. Zeelenberg, A. J. J. Bos, K. W. Kramer, and P. Dorenbos, J. Appl. Phys. **104**, 073505 (2008).
[25] R. Chen and S. W. S. McKeever, *Theory of Thermoluminescence and Related Phenomena* (World Scientific, Singapore, 1997).
[26] M. Puchalska and P. Bilski, Radiat. Meas. **41**, 659 (2006).
[27] P. Dorenbos, J. Lumin. **108**, 301 (2004).
[28] R. J. Lang, Can. J. Res., Sect. A **14**, 127 (1936).
[29] P. Dorenbos, J. Phys.: Condens. Matter **15**, 4797 (2003).
[30] P. Dorenbos, J. Lumin. **104**, 239 (2003).